SCIENCE CHINA
Physics, Mechanics & Astronomy

• Research Paper •

August 2010 Vol.53 No.8: 1466–1474
doi: 10.1007/s11433-010-4063-5

Temperature pattern dynamics in shocked porous materials

XU AiGuo*, ZHANG GuangCai, LI Hua, YING YangJun, YU XiJun & ZHU JianShi

National Key Laboratory of Computational Physics, Institute of Applied Physics and Computational Mathematics, Beijing 100088, China

Received September 17, 2009; accepted November 23, 2009

The physical fields in porous materials under strong shock wave reaction are very complicated. We simulate such systems using the grain contact material point method. The complex temperature fields in the material are treated with the morphological characterization. To compare the structures and evolution of characteristic regimes under various temperature thresholds, we introduce two concepts, structure similarity and process similarity. It is found that the temperature pattern dynamics may show high similarity under various conditions. Within the same material, the structures and evolution of high-temperature regimes may show high similarity if the shock strength and temperature threshold are chosen appropriately. For process similarity in materials with high porosity, the required temperature threshold increases parabolically with the impact velocity. When the porosity becomes lower, the increasing rate becomes higher. For process similarity in different materials, the required temperature threshold and the porosity follow a power-law relationship in some range.

porous material, shock wave, characteristic regimes, material point method, morphological analysis

PACS: 05.70.Ln, 05.70.-a, 05.40.-a

Inhomogeneous materials are ubiquitous in nature and extensively used as industrial materials [1]. Besides the granular materials [2,3], porous materials have long been used to protect things from strong impact. The inhomogeneity of the material may change significantly its shock response behaviors. When being reacted by a weak shock, the embedded cavity in the material may result in a secondary impact; When being reacted by a strong shock, jet phenomena may occur at the cavity [4,5]. Globally speaking, shock wave reaction results in various characteristic regimes, for example, "high pressure regimes", "high temperature regimes", "regimes with high particle speeds", "regimes with high deviatoric stresses", etc. These regimes are places where problems may occur in practical applications. For example, phase transition may occur in the high pressure regimes, plastic deformation may occur in the regimes with high deviatoric stresses, jet phenomena may occur in regimes with high particle speeds, chemical reaction may occur in the high temperature regimes if the material is energetic. These phenomena can also be functioning if properly controlled. The structure, distribution and evolution of these regimes should be carefully studied. Although the study on shock wave reaction has a long history, most of previous studies were focused on some global behaviors, such as the Hugoniots [6] and equations of state [7]. To get relevant physical information for shock wave response of porous materials, Xu et al. [8] introduced the Minkowski functionals to characterize the distribution and evolution of physical fields in the materials. Procedures with shock wave reaction on porous materials is generally related to large distortion and very strong nonlinearity. The theoretical description of such a system is a very difficult issue. From the experimental side, the measurements of very quick processes and detailed dynamics are also challenging. Therefore, numerical simulations play an indisplaceable role in providing a complete understanding. From the simulation side, both the scales and numerical stability should be considered. The molecular dynamics may discover some microscopic mechanisms for the cavity collapse and occurrence of disloca-

*Corresponding author (email: Xu_Aiguo@iapcm.ac.cn)

tions. But the scales it can access are still much less than microsecond and micrometer. It is too small to be comparable with experiments [9,10]. When use the traditional Lagrangian and Eulerian algorithms to treat with such problems, they generally encounter severe difficulties. The Lagrangian methods can capture well the material interfaces but have problems of large mesh deformation. In Eulerian methods, the background meshes are fixed in space. But such a scheme is not easy to track interfaces. In order to combine the merits of the Lagrangian and Eulerian schemes and avoid their drawbacks, we use a mixed method, the Material Point Method (MPM) [11,12], to investigate the dynamical procedure of shock wave reaction on porous materials.

1 Material model and numerical schemes

1.1 Material model

In our simulations, the porous material is fabricated by a solid body with an amount of randomly distributed voids embedded. The solid portion follows an associative von Mises plasticity model with linear kinematic and isotropic hardening [4]. The material shows a linear elastic response until the von Mises yield criterion is reached. The yield criterion reads $3J_2-\sigma_Y^2=0$, where σ_Y is the plastic yield stress,

$$J_2=\frac{1}{2}\boldsymbol{S}:\boldsymbol{S} \tag{1}$$

is the second invariant of the deviatoric stress tensor,

$$\boldsymbol{S}=\boldsymbol{\sigma}-\frac{1}{3}\mathrm{Tr}[\boldsymbol{\sigma}]. \tag{2}$$

The linear hardening means that the plastic yield stress increases linearly with the second invariant of the plastic strain tensor. When $J_2>{\sigma_Y}^2$, the increment of equivalent plastic strain $\mathrm{d}\varepsilon_p$ can be calculated as

$$\mathrm{d}\varepsilon_p=(\sqrt{3J_2}-\sigma_Y)/(3G+E_{\tan}), \tag{3}$$

where G and $E_{\tan}$ are the shear and hardening modulus, respectively. We assume that the increment of plastic work, $\mathrm{d}W_P=\mathrm{d}\varepsilon_P\cdot\sigma_Y$, is totally transformed into heat. The pressure P follows the Mie-Gruneissen equation of state [13–16]

$$P-P_H=\frac{\gamma(V)}{V}[E-E_H(V_H)], \tag{4}$$

where P_H, V_H and E_H are the pressure, specific volume and energy on the Rankine-Hugoniot curve, respectively. The pressure P_H is related to the specific volume V_H by the following relation:

$$P_H=\begin{cases}\dfrac{\rho_0{c_0}^2\left(1-\dfrac{V_H}{V_0}\right)}{(\lambda-1)^2\left(\dfrac{\lambda}{\lambda-1}\times\dfrac{V_H}{V}-1\right)^2}, & V_H\leqslant V_0,\\ \rho_0{c_0}^2\left(\dfrac{V_H}{V_0}-1\right), & V_H>V_0,\end{cases} \tag{5}$$

where c_0 is the sound speed, λ is the coefficient in the Hugoniot velocity relation $U_S=c_0+\lambda U_P$, U_S is the velocity of the shock wave, U_P is the particle speed after the shock [16]. In this work, the Gruneissen coefficient γ is a constant, the specific energy $(E-E_H)$ is the plastic work. Both the shock compression and plastic work lead to the increasing of temperature. The increment of temperature by shock compression is calculated by

$$\frac{\mathrm{d}T_H}{\mathrm{d}V_H}=\frac{{c_0}^2\lambda(V_0-V_H)^2}{c_v[(\lambda-1)V_0-\lambda V_H]^3}-\frac{\gamma(V)}{V_H}T_H, \tag{6}$$

where c_v is specific heat [16]. The temperature increment by plastic work is calculated by

$$\mathrm{d}T_p=\frac{\mathrm{d}W_p}{c_v}. \tag{7}$$

In this study the example material is porous aluminum. The material parameters are as follows: the initial density in solid portion $\rho_0=2700$ kg/m^3, elastic modulus E=69 GPa, Poisson ratio ν=0.33, initial yield strength σ_{Y0}=120 MPa, hardening modulus $E_{\tan}=384$ MPa, sound speed c_0= 5350 m/s, specific heat $c_v=880$ J/(kg K), heat conduction coefficient $k=237$ W/(m K). In our simulations, the shock wave on porous material is loaded by colliding with a rigid wall being static at the bottom. The impact starts at the time t=0. The impact velocity is $-V$. Periodic boundary conditions are used in the horizontal direction. In this work, we focus on the two-dimensional simulations. The initial temperature of the system is 300 K.

1.2 Numerical method

As a particle scheme, the material point method discretizes the continuous portion of the body as N_P material particles or material points. Each material particle carries the mass m_P, stress $\boldsymbol{\sigma}_P$, speed $\boldsymbol{v}_P$, density ρ_P, etc. all relevant material information. This method uses an Eulerian background mesh. Each mesh node carries the information of velocity $\boldsymbol{v}_i$ and acceleration $\boldsymbol{a}_i$, where i is the index of mesh node. At each time step, the material particles flow in space according to the deformation of the material body.

Then map the material information from material particles to mesh nodes. Calculate the spatial derivatives and integrate the momentum equation at the mesh nodes. The updated node velocity $\boldsymbol{v}_i$ and acceleration $\boldsymbol{a}_i$ are mapped back to the material particles. The information of material particles at next step is updated. In our simulations, the background mesh are predefined and fixed. So, there is no mesh entangling problems.

The fundamental theory of MPM is as below: In MPM the mass of each material particle is fixed, so the continuity equation:

$$\frac{\mathrm{d}\rho}{\mathrm{dt}} + \rho\nabla\cdot\boldsymbol{v} = 0 \tag{8}$$

is automatically satisfied, where ρ is the mass density, $\boldsymbol{v}$ is the local velocity. The mechanical equilibrium equation in the Lagrangian frame reads,

$$\rho\frac{\mathrm{d}\boldsymbol{v}}{\mathrm{d}t} = \nabla\cdot\boldsymbol{\sigma} + \rho\boldsymbol{b} = 0, \tag{9}$$

where $\boldsymbol{b}$ is the body force. At each simulation step, the mass and velocity of material particles are mapped on the background mesh nodes. The node velocity is calculated by

$$\sum_j m_{ij}\boldsymbol{v}_j = \sum_p m_p\boldsymbol{v}_p N_i(\boldsymbol{x}_p), \tag{10}$$

where N_i is the shape function, $\boldsymbol{x}_P$ is the position of material particle *P*. A weak form of eq. (9) reads

$$\int_\Omega \rho\delta\boldsymbol{v}\cdot\frac{\mathrm{d}\boldsymbol{v}}{\mathrm{d}t}\mathrm{d}\Omega + \int_{\Gamma_t}\rho\delta\boldsymbol{v}\cdot(\boldsymbol{\sigma}\cdot\boldsymbol{n}-\boldsymbol{t})\mathrm{d}\Gamma + \int_\Omega \rho\delta\boldsymbol{v}\cdot\boldsymbol{b}\mathrm{d}\Omega = 0, \tag{11}$$

where Ω is the domain for solution, Γ_t is the force boundary, $\boldsymbol{t}$ is the external force. Since being discretized as a group of material particles, the mass density can be written as

$$\rho(\boldsymbol{x}) = \sum_p m_p\delta(\boldsymbol{x}-\boldsymbol{x}_p). \tag{12}$$

Substituting eq. (12) into (11) gives

$$m_i\frac{\mathrm{d}v_i}{\mathrm{d}t} = f_i^{\mathrm{int}} + f_i^{\mathrm{ext}}, \tag{13}$$

where $\boldsymbol{f}_i^{\mathrm{int}}$ and $\boldsymbol{f}_i^{\mathrm{ext}}$ represents vectors of the internal and external forces, respectively. Their expressions are as follows:

$$\boldsymbol{f}_i^{\mathrm{int}} = -\sum_P\frac{1}{\rho_P}m_P\boldsymbol{\sigma}\cdot(\nabla N_i), \tag{14}$$

$$\boldsymbol{f}_i^{\mathrm{ext}} = \sum_P N_i\boldsymbol{b}_P + \boldsymbol{f}_i^C. \tag{15}$$

In eq. (15) vector $\boldsymbol{f}_i^C$ represents the contact force and external boundary force. Equation (13) can be calculated by an explicit time integration scheme. The contact algorithm is the core of a MPM. What we used here is an improved one given in recent literature [5]. The MPM combined with the contact algorithm in ref. [5] is also referred to Grain Contact Material Point Method (GCMPM).

2 Morphological analysis

Shock wave reaction results in very complicated spatio-temporal structures inside the porous body. The distribution and evolution of physical fields are very complex. The data analysis for such a system is generally resort to statistical schemes. In this work, we focus on a set of statistics named Minkowski functionals [8]. The Minkwoski functionals describe the patterns of physical field from the morphological side.

Assume Ω is a physical variable under consideration, Ω_{th} is a given threshold value, where Ω can be the density, pressure, temperature, particle velocity, deviatoric stress, etc. In morphological analysis, the regimes with $\Omega \geqslant \Omega_{\mathrm{th}}$ are defined as white, other regimes are defined as black. In this way, nearly all the continuous patterns can be decomposed of a collection of white and black pixels. A set of neighboring white or black pixels compose of a white or black domain. Minkowski functionals or morphological analysis presents a set of complete descriptions for such a Turing pattern satisfying motion invariance and additivity. For *D*-dimensional patterns, the number of the Minkowski functionals is *D*+1. In the two-dimensional case, a physical filed $\Omega(\boldsymbol{x})$ presents a two-dimensional map, where $\boldsymbol{x}$ denotes the position in the material body. We need three Minkowski functionals to characterize its morphological properties. The three Minkowski functionals are the fractional white area *A*, the fractional boundary length *L* and the Euler characteristic χ. The Euler characteristic is also referred to the connectivity. It describes the morphological properties of a pattern from the pure topological way. The three functionals possess additivity, motion invariance and continuity. The Minkowski functionals can be very helpful in analyzing complicated physical processes.

In this work we analyze the pattern dynamics of the temperature field $T(\boldsymbol{x})$ in the shocking procedure. The above white area corresponds to high temperature area. The black area corresponds to low temperature area. Those scattered white pixels corresponds to small "hot spots" occurring inside the material. Although the three functionals describe global behaviors of a map, they can be calculated in some local way. The fractional white area A is defined as

$A = N^W / N$, where N^W is the number of white pixels and N is the number of total pixels. It is clear that when temperature threshold T_{th} increases from the lowest temperature $T_{\min}$ to the highest temperature $T_{\max}$ in the system, the fractional white area A decreases from 1 to zero. The fractional boundary length L is calculated as $L=B/N$, where B is the total boundary length separating the white and black areas. When temperature threshold T_{th} increases from $T_{\min}$ to $T_{\max}$, the fractional boundary length L increases from zero and finally decreases to zero; at some specific temperature threshold, the boundary length gets its maximum value. The Euler characteristic $\chi = (n^W - n^B)/N$, where n^W and n^B are numbers of the white and black domains inside the material. When the number of white domains dominates, $\chi > 0$; else $\chi < 0$.

We can consider the morphological properties of two patterns in the three- dimensional space opened by the three Minkowski functionals, A, L and χ. Each pattern is denoted by one point in the A–L–χ space. Since all the morphological properties of a two-dimensional pattern are contained in the three Minkowski functionals, if the two points coincide, then the morphological properties of the two patterns are the same; if the two points are very close, then the morphological properties of the two patterns are very similar; the farther the two points, the less similar the two patterns. A temperature Turing pattern gives a structure of the high temperature regimes in the material body. Therefore, we can define a pattern similarity or structure similarity S as follows:

$$S = \frac{1}{d}, \tag{16}$$

where $d = \sqrt{(A_2 - A_1)^2 + (L_2 - L_1)^2 + (\chi_2 - \chi_1)^2}$ is the distance between pattern 1 and pattern 2 in the A–L–χ space. If the two patterns evolve with time from t_1 to t_2, then we can define a process similarity S_P as below:

$$S_P = \frac{1}{d_P}, \tag{17}$$

where

$$\mathrm{d}_P = \frac{1}{t_2 - t_1}\int_{t_1}^{t_2} \mathrm{d}(t)\mathrm{d}t \tag{18}$$

is the mean distance between the two pattern dynamical procedures. For convince of description, we define $DT = T_{\text{th}}$–300.

3 Results of numerical experiments

3.1 Case with porosity 0.077 and impact velocity 1100 m/s

Figure 1 shows a set of snapshots for the shocking procedure on the porous aluminum. The points in the snapshots corresponds to material particles. The color, from black to white, corresponds to the increase of temperature. The height and width of the simulated material body are 5 and 1 mm, respectively. The porosity here is Δ=0.077, the initial impact velocity between the porous aluminum and bottom is V=1100 m/s. From left to right, the four snapshots are for the times t=500, 750, 850 and 1100 ns, respectively. The former two snapshots are for the shock loading procedure, the latter two are for the shock unloading procedure. From the snapshots, it is clear that the situation is greatly different from the case with solid uniform materials. In the case with uniform materials, the shock front is a plane and the system after the shock is in an uniform equilibrium state. But here the initial shock wave is decomposed as a very complicated series of compressive waves and tensional waves. In the shock loading procedure, the compression effects dominate. In the region scanned by compressive waves, the temperature of material particles increase. The interface between the portions with higher temperatures and the portion with original temperature gives the shock front. It is much wider than that in the case with uniform materials. The physical reason is as below. When the initial shock wave meets with a cavity inside the material body, the cavity reflects tensional waves back into the compressed portion; the compressive waves at the two sides of the cavity propagate forwards and collide in the front of the cavity; if the shock is strong enough, the cavity collapses and jet phenomenon occurs. When the jet material particles hit the downstream wall of the cavity, it results in a secondary shock loading. Up to this step, the original simple shock wave has been transformed into complex wave series. When these waves meet with a second, third cavities, the waves become much more complex. These phenomena continue to occur in the downstream portion of the material. At the same time, mechanical energy is transferred upwards from the impact plane continuously before the end of the shock loading procedure. The new mechanical energy results in new compression and plastic work. Thus, during the whole shock

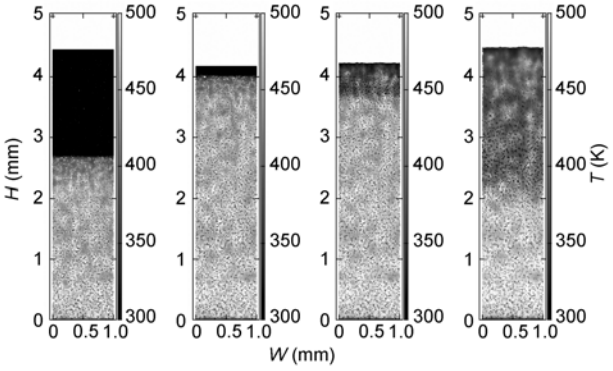

Figure 1 A set of configurations with temperature contour in the shock loading and unloading procedure.

loading procedure, the system scanned by the waves is in a nonequilibrium state. The distribution of density, pressure, temperature, particle velocities, etc. are very complicated.

Greatly different from the case with solid uniform materials, the temperature increase in shocked porous materials result from, at least, two fundamental mechanisms: isoentropic compression and plastic work. The former is similar to the effect of ideal gas. When tensional waves come, the pressure decreases, the temperature decreases, too. The latter is entropy increasing process. It is irreversible. When tensional waves come, the pressure decreases, but the tensional waves may contribute plastic work; in such a case, the temperature will increase further. In the case shown in Figure 1, the porosity is very low, the situation is very close to that of uniform material. The coming in of tensional waves from the upper free surface leads to a significant decrease of temperature.

Figure 2 presents a set of morphological analysis for the dynamical process shown in Figure 1. From upper to down, the three plots show the fractional high temperature area A versus time t, the boundary length L versus time t, the Euler characteristic χ versus time t. The numbers shown in the legend are values of $T_{\text{th}} - 300$. The unit is K. The first plot shows that the high temperature areas $A(t)$ for $T_{\text{th}} - 300 = 50$ and $T_{\text{th}} - 300 = 100$ increase with time in nearly the same way. They arrive at 1.0 at about the time $t = 750$ ns. This means that nearly all the materials particles scanned by the compressive waves have a temperature increment higher than 100 K. At the initial period of shock unloading, the $A(t)$ curve for $T_{\text{th}} - 300 = 100$ decreases more quickly than that for $T_{\text{th}} - 300 = 50$. This result shows quantitatively that the reflected tensional waves result in the decrease of pressure, and consequently the decrease of temperature of some material particles. This result shows also a piece of very important information: the decreasing of temperature in shocked porous materials is much slower than in shocked uniform materials. During the shock loading procedure, with the increase of temperature threshold, the increasing rate of high temperature area decreases. At the end of shock loading, there are 82% material particles get a temperature increment higher than 150 K, 31% material particles get a temperature increment higher than 200 K, only 7% material particles get a temperature increment higher than 250 K. Among the cases shown in Figure 2, the $A(t)$ curve decreases most quickly during the initial period of shock unloading.

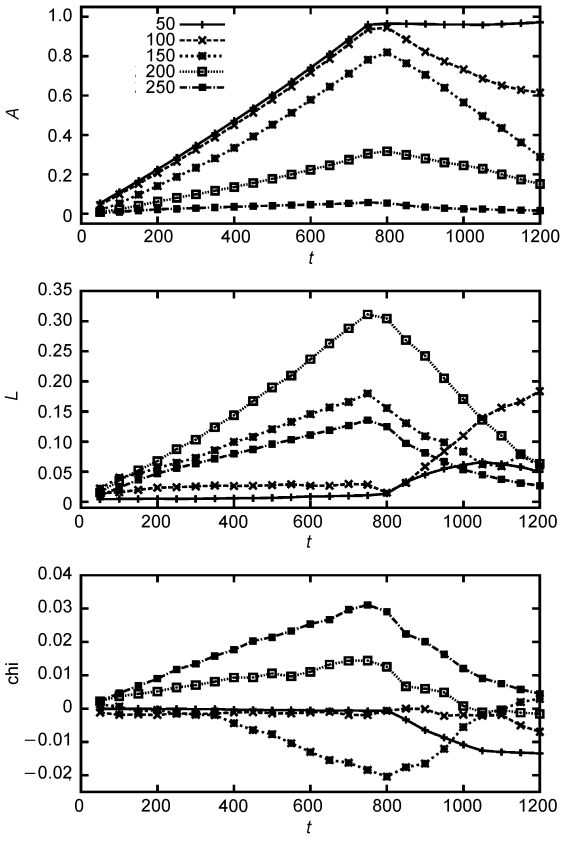

Figure 2 Morphological analysis for the procedure of shock wave reaction on porous material.

Now we go to the evolution of boundary length $L(t)$. When $T_{\text{th}} - 300 = 50$ K, the boundary length $L(t)$ keeps very small during the whole shock loading procedure. When $T_{\text{th}} - 300 = 100$ K, the boundary length $L(t)$ has a slight increase. This slight difference indicates that there are a very small amount of material particles have a temperature between 350 and 400 K. When the value of $T_{\text{th}} - 300$ increases up to 150 and 200 K, the boundary length $L(t)$ increases further. This increase means that the number of low-temperature material particles increases, the domains with low-temperature material particles become large. If further increase the temperature threshold T_{th} to 550 K, the boundary length $L(t)$ will show different behavior, it will decrease. This decrease means that the area of low temperature has been dominating and become the background, the high temperature spots becomes small and scattered. Since the boundary length for $T_{\text{th}} - 300 = 100$ and $T_{\text{th}} - 300 = 50$ keeps very small during the whole shock loading procedure, they increase during the initial shock unloading procedure. Other boundary lengths begin to decrease quickly when the unloading starts.

The Euler characteristic $\chi(t)$ presents the connectivity of the high temperature domains and low temperature domains in the temperature Turing pattern. When $T_{\text{th}} - 300 =$ 50 and 100, the connectivity is the best, so $\chi(t)$ is very close to zero during the shock loading procedure. When $T_{\text{th}} - 300 = 150$, except for the initial loading period, the value of $\chi(t)$ becomes more negative with time during the loading procedure. This behavior shows that the number of

low temperature domains increases more quickly than that of high temperature domains. When $T_{\text{th}}-300=200$ and 250, the number of high temperature domains becomes more dominative with time during the shock loading procedure. But the situation changes when the shock unloading starts.

Figure 3 shows a set of morphological analysis in the A–L–χ three dimensional space. Figure 3 is equivalent to Figure 2 except for that the time t is not explicitly labeled here. In the shock loading procedure, with the increase of the high temperature area A, a point in the curve corresponds to a measuring time. During the initial period of shock unloading, the high temperature area A decreases. Since the two curves, for $T_{\text{th}}-300=50$ and $T_{\text{th}}-300=100$, keep close during the shock loading procedure. This keeping close means that the two temperature Turing pattern dynamical processes show high similarity.

3.2 Similarities in the same material

We check the process similarities in temperature Turing pattern dynamics for the same material under various shock strengths. Since the porosity Δ is fixed, a Turing pattern dynamics is labeled by a pair of parameters, the initial impact velocity V and the temperature threshold $DT(V)$. The reference process is labeled by the initial impact velocity $V=1100$ m/s and the temperature threshold $DT(V=1100)$. Shocking processes with various impact velocities are compared with the reference process. Their distances to the reference process are calculated. The reciprocal of a distance d_P gives the process similarity S_P.

We first consider the case with low porosity. In Figure 4(a) the porosity is $\Delta=0.077$, $DT(V=1100)=120$ K. The vertical axis shows the reciprocal of process similarity, d_P. The horizontal axis shows the temperature threshold, $T_{\text{th}}-300$. Comparison results for initial impact velocities, 700, 900, 1000, 1100, 1200, 1300, 1400 and 1500 m/s, are shown. It is clear that, when the initial impact velocity is 1100 m/s, the d_P curve has a minimum, 0, at $DT=120$ K. Each of other curves has also a minimum. The corresponding horizontal coordinate gives the temperature threshold for the most similar pattern dynamical process. For example, we can find that the dynamical process for (1100 m/s, 120 K)and that for (1000 m/s, 92 K) show high similarity, that the dynamical process for (1100 m/s, 120 K) and that for (1200 m/s, 154 K) show also high similarity. To observe more detailed information, we show the three pattern dynamical procedures in the A–L–χ space in Figure 5. The number pairs shown in the legend give the initial impact velocity and the value of $T_{\text{th}}-300$. Their units are m/s and K, respectively. It is clear that the two curves for (1000 m/s, 92 K) and (1200 m/s, 154 K) locate at the two sides of the one for (1100 m/s, 120 K). At the initial period of the shock loading procedure, they three are nearly the same; the differences between any two of them increases slightly with the propagation of compressive waves in the porous material. But during the whole period shown in Figure 5, they three keep very near. The other minimum points in Figure 4(a) present similar information and can be analyzed in a similar way. Since nearly all the morphological properties

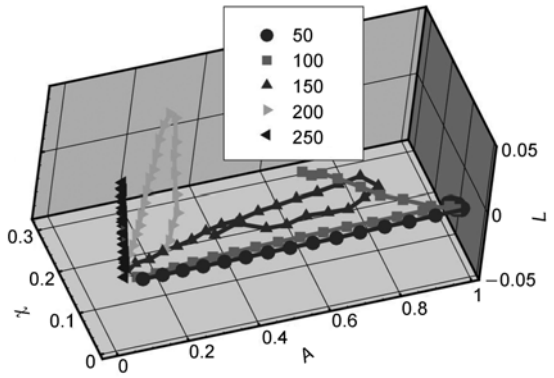

Figure 3 Morphological analysis in the A–L–χ space.

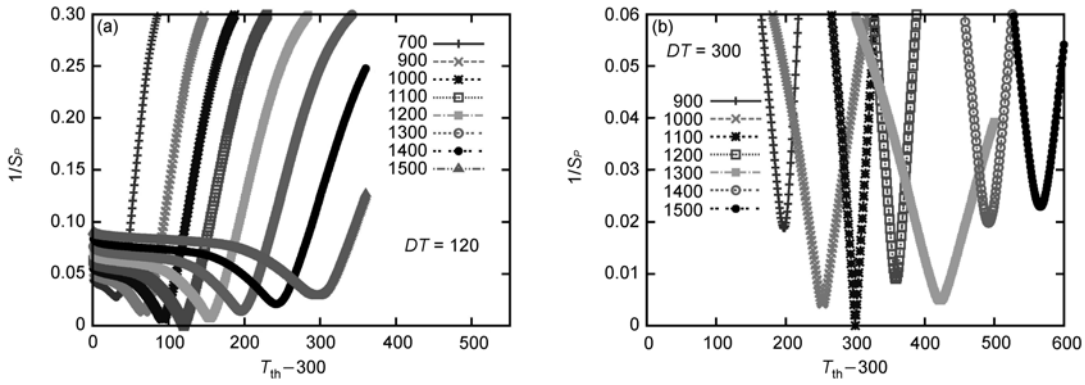

Figure 4 Process similarity versus temperature threshold.

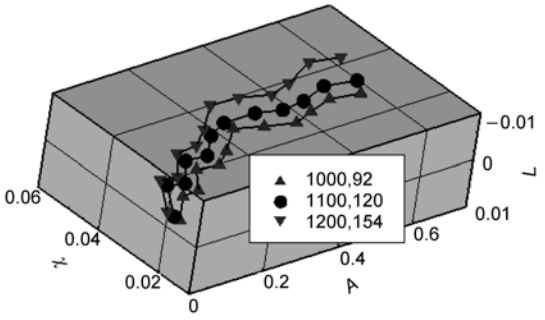

Figure 5 Three similar pattern dynamical procedures in the A–L–χ space.

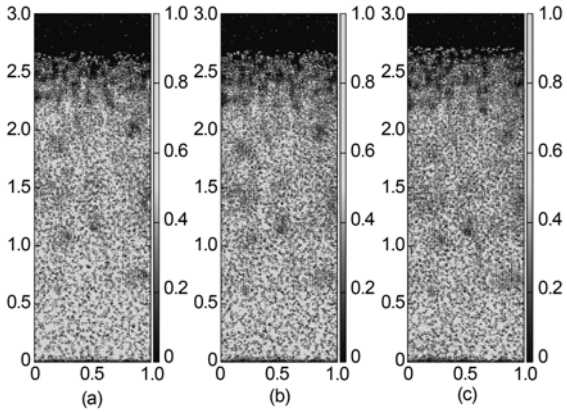

Figure 6 Condensed temperature patterns at time 500 ns in the three similar dynamical procedures.

of the two-dimensional temperature Turing pattern are condensed into one point in the A–L–χ space, the information we can get from Figure 5 is still a little abstruse. To see more clearly how similar the three pattern dynamical procedures are, we show the condensed temperature Turing patterns at the time $t = 500$ ns for the three dynamical procedures in Figure 6, where the material particles have only two color levels, those with a temperature higher than the threshold value are shown in gray and others are shown in black. (The time $t = 500$ ns corresponds to the 10^{th} point of each curve along the direction of increasing A.) The initial impact velocity and the value of $T_{\text{th}} - 300$ are (1000 m/s, 92 K), (1100 m/s, 120 K) and (1200 m/s, 154 K), respectively, in Figures 6(a)–(c).

Simulation results show also that, the stronger the initial shock strength, the higher the temperature threshold. If use the pairs of temperature threshold DT and the impact velocity V for the most similar pattern dynamics to compose a curve, we get the curve in Figure 5(a) and labeled with "120". In Figure 5, the horizontal axis shows the shock strength manifested by V^2/10000 and the vertical axis shows the temperature threshold, $T_{\text{th}} - 300$. If choose different values for $DT(V = 1100)$, for example, 150, 180, and 200, then we get the other curves shown in Figure 5(a).

For cases with high porosity, we show an example in Figure 4(b). In Figure 4(b) the porosity is $\Delta = 0.46$. The temperature threshold for the reference process is $DT(V = 1100) = 300$ K. Figure 4(b) shows the comparison results for initial impact velocities, 900, 1000, 1100 m/s, 1200, 1300, 1400, and 1500 m/s. The closer the initial impact velocity to 1100 m/s, the closer the value of DT to 300 K. If use the pairs of DT and impact velocity V to compose a curve, we get the one in Figure 7(b) and labeled with "300". If choose different temperature thresholds, for example, $DT(V = 1100) = 280$, 320, 350, and 380, repeat the above processes, we get the curves labeled with "280", "320", "350" and "380" in Figure 7(b).

Comparison of Figures 7(a) and 7(b) indicates that, when the porosity is high, the temperature threshold T_{th} increases parabolically with the initial impact velocity V; with the decreasing of the porosity, the increasing rate becomes higher. The physical reason is as below: When the porosity is high, between the two fundamental mechanisms for heat creation, the plastic work dominates; With the decreasing of the porosity, the shocking behavior becomes more close to that of solid uniform material; the contribution of plastic work decreases while the isoentropic compression effect

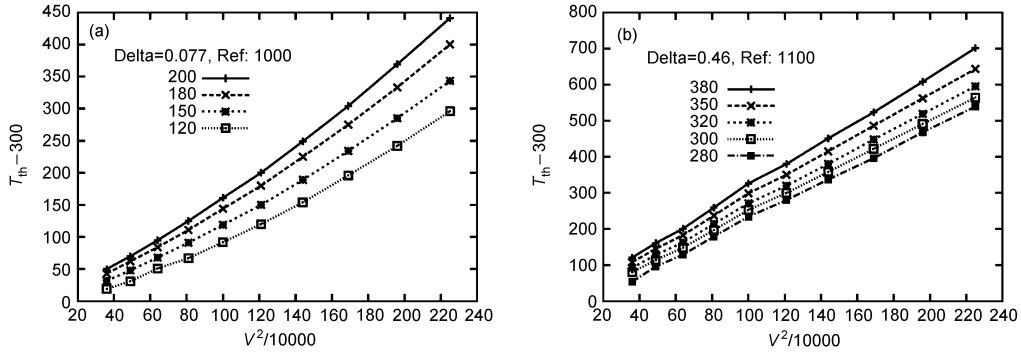

Figure 7 Temperature threshold versus shock strength.

contributes relatively more.

3.3 Dynamical similarities in different materials

We check the temperature Turing pattern dynamics in materials with various porosities under shock wave reaction. For the convenience of comparison, we fix the shock strength. Thus, a Turing pattern dynamics is labeled by two parameters, the porosity Δ and the corresponding temperature threshold $DT(\Delta)$. Figure 8 shows a set of examples. Here, the fixed initial impact velocity is $V = 1100$ m/s. The reference dynamical process is labeled by the porosity $\Delta = 0.077$ and the temperature threshold $DT(\Delta = 0.077)$. When the reference temperature threshold $DT(\Delta = 0.077)$ = 300 K, we check the temperature Turing pattern dynamics in shocking procedures with various porosities Δ and temperature thresholds DT. Compare the distances between them to the reference process, pick out the $DT(\Delta)$ values for the highest process similarities. Use the values of porosity Δ and corresponding DT to compose a curve, we get the curve in Figure 8 and labeled by "300". Curves for some other $DT(\Delta = 0.077)$ values are also shown. This figure is in $\ln \sim \ln$ scale. The simulation results show that the temperature threshold DT increases with the porosity Δ. In an appropriate range, they follows nearly a power-law relationship. For a fixed shock strength, when the porosity is high enough, the power-law relation breaks.

4 Summary and conclusion

Greatly different from the case with uniform materials, under strong shock wave reaction, various characteristic regimes will occur in porous materials. Examples are referred to high pressure regimes, high temperature regimes, regimes with high particle speeds, regimes with high deviatoric stresses, etc. These regimes are generally problematic and/or functioning in practical applications. For example, phase transition may occur in high pressure regimes, plastic deformation may occur in regimes with high deviatoric stress, jet phenomena may occur in regimes with high particle speeds, chemical reaction may occur in the high temperature regimes if the material is energetic. To use or control better these phenomena, the structure and evolution of these kinds of characteristic regimes should be carefully investigated.

We simulate such systems via the grain contact material point method. Use the Minkowski functionals to characterize the temperature map from the morphological side. Two new concepts, structure similarity and process similarity, are defined to search some fundamental and common properties in such systems. It is found that, the temperature pattern dynamics may show high similarity under various conditions. Within the same material, if the shock strength and temperature threshold are chosen appropriately, the temperature Turing pattern dynamics will show high similarity. When the porosity is high, the temperature threshold for highest similarity increases parabolically with the initial impact velocity. With the decrease of material porosity, the increasing rate becomes higher. For similarities in different materials, under the same shock strength, the temperature threshold for highest similarity and the porosity show a power-law relationship in some range. These results deepen the understanding on porous material under shock wave reaction and present some helpful information for designs of relevant experiments. Other kinds of characteristic regimes can be studied in the same way.

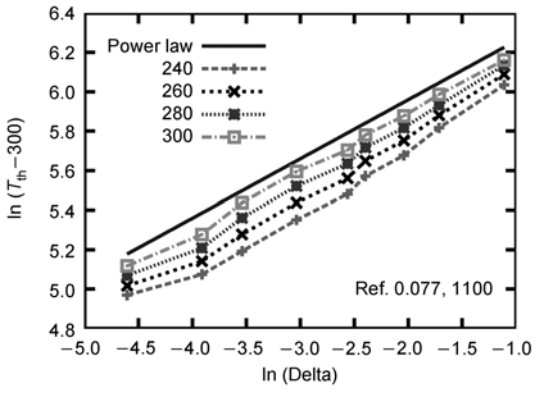

Figure 8 Temperature threshold versus porosity.

The authors would like to thank Profs. ZHANG Ping, WANG Jianguo, XU HaiBo, LIU XingPing, et al. for helpful suggestions and discussions. This work was supported by the National Natural Science Foundation of China (Grant Nos. 10702010, 10775018, and 10771019), Science Foundation of Laboratory of Computational Physics and Science Foundation of China Academy of Engineering Physics (Grant Nos. 2009A0102005 and 2009B0101012).

1 Nesterenko V F. Dynamics of Heterogeneous Materials. New York: Springer-Verlag, 2001
2 Hong J, Xu A G. Effects of gravity and nonlinearity on the waves in the granular chain. Phys Rev E, 2001, 63: 061310-1–7
3 Hong J, Xu A G. Nondestructive identification of impurities in granular medium. Appl Phys Lett, 2002, 81: 4868–4870
4 Xu A G, Pan X F, Zhang G C, et al. Material-points imulation of cavity collapse under shock. J Phys-Condens Matter, 2007, 19: 326212
5 Pan X F, Xu A G, Zhang G C, et al. Generalized interpolation material point approach to high melting explosive with cavities under shock. J Phys D-Appl Phys, 2008, 41: 015401
6 Butcher B M, Carroll M M, Holt A C. Shock-wave compaction of porous aluminum. J Appl Phys, 1974, 45: 3864–3875
7 Wu Q, Jing F Q. Unified thermodynamic equation-of-state for porous materials in a wide pressure range. Appl Phys Lett, 1995, 67: 49–51
8 Xu A G, Pan X F, Zhang G C, et al. Morphological characterization of shocked porous material. J Phys D-Appl Phys, 2009, 42: 075409
9 Yang Q L, Zhang G C, Xu A G, et al. Molecular dynamics simulations of shock induced colapse in single crystal copper with na-

nano-void inclusion. Acta Phys Sin, 2008, 57: 940–946
10 Fang B Q, Lu G, Zhang G C, et al. Evolution of stacking-fault-tetrahedron-like structures in copper crystal. Acta Phys Sin, 2009, 58: 4862–4871
11 Pan X F, Xu A G, Zhang G C, et al. Three-dimensional multi-mesh material point Method for solving collision problems. Commun Theor Phys, 2008, 49: 1129–1138
12 Ma S, Zhang X, Qiu X M. Comparison study of MPM and SPH in modeling hypervelocity impact problems. Int J Impact Eng, 2009, 36: 272–282
13 Xu X S, Zhang W X. Introduction to Practical Equation of State. Beijing: Science Press, 1986. 418–446
14 Sun J S, Zhu J S. Theoretical Explosion Physics. Beijing: National Defence Industry Press, 1995. 88–134
15 Zhang G R, Chen D N. Initiation Dynamics of Condensed Explosives. Beijing: National Defence Industry Press, 1991. 35–37
16 Zhang B P, Zhang Q M, Huang F L. Explosion Physics. Beijing: Ordnance Industry Press, 2001. 375–391